# Tailoring the Pharmacokinetics and Positron Emission Tomography Imaging Properties of Anti–Carcinoembryonic Antigen Single-Chain Fv-Fc Antibody Fragments

Vania Kenanova,[1,6] Tove Olafsen,[6] Desiree M. Crow,[3] Gobalakrishnan Sundaresan,[6] Murugesan Subbarayan,[7] Nora H. Carter,[5] David N. Ikle,[5] Paul J. Yazaki,[3] Arion F. Chatziioannou,[6] Sanjiv S. Gambhir,[7] Lawrence E. Williams,[4] John E. Shively,[2] David Colcher,[3] Andrew A. Raubitschek,[3] and Anna M. Wu[1,6]

Divisions of [1]Molecular Biology and [2]Immunology, Beckman Research Institute of the City of Hope; [3]Department of Radioimmunotherapy, [4]Radiology Division, and [5]Department of Biostatistics, City of Hope National Medical Center, Duarte, California; [6]Crump Institute for Molecular Imaging, Department of Molecular and Medical Pharmacology, David Geffen School of Medicine at University of California, Los Angeles, California; and [7]Department of Radiology and Bio-X Program, Stanford University School of Medicine, Stanford, California



## Abstract

**Antibody fragments are recognized as promising vehicles for delivery of imaging and therapeutic agents to tumor sites *in vivo*. The serum persistence of IgG1 and fragments with intact Fc region is controlled by the protective neonatal Fc receptor (FcRn) receptor. To modulate the half-life of engineered antibodies, we have mutated the Fc-FcRn binding site of chimeric anti–carcinoembryonic antigen (CEA) antibodies produced in a single-chain Fv-Fc format. The anti-CEA T84.66 single-chain Fv-Fc format wild-type and five mutants (I253A, H310A, H435Q, H435R, and H310A/H435Q, Kabat numbering system) expressed well in mammalian cell culture. After purification and characterization, effective *in vitro* antigen binding was shown by competition ELISA. Biodistribution studies in BALB/c mice using $^{125}$I- and $^{131}$I-labeled fragments revealed blood clearance rates from slowest to fastest as follows: wild-type > H435R > H435Q > I253A > H310A > H310A/H435Q. The terminal half-lives of the mutants ranged from 83.4 to 7.96 hours, whereas that of the wild-type was ~12 days. Additionally, $^{124}$I-labeled wild-type, H435Q, I253A, H310A, and H310A/H435Q variants were evaluated in LS174T xenografted athymic mice by small animal positron emission tomography imaging, revealing localization to the CEA-positive xenografts. The slow clearing wild-type and H435Q constructs required longer to localize to the tumor and clear from the circulation. The I253A and H310A fragments showed intermediate behavior, whereas the H310A/H435Q variant quickly localized to the tumor site, rapidly cleared from the animal circulation and produced clear images. Thus, attenuating the Fc-FcRn interaction provides a way of controlling the antibody fragment serum half-life without compromising expression and tumor targeting.** (Cancer Res 2005; 65(2): 622-31)

## Introduction

Monoclonal antibodies and antibody fragments are not new to the pharmacology arena in both cancer treatment and imaging. Although favorable in terms of stability, target affinity, and specificity, native antibodies are noted for their prolonged serum half-life. Thus, a problem arises when intact antibodies are conjugated to radionuclides or other toxic agents. Because immunoglobulin G (IgG) remains in circulation for extended periods of time, the conjugate can cause significant irradiation and toxicity to normal organs, such as the bone marrow, liver, and kidneys. This would translate to reduced therapeutic dose, less frequent administrations, and ultimately compromised pharmacologic feasibility.

Currently, the most common approach for minimizing antibody circulation persistence is reduction in size by deletion of domains. Several laboratories, including our own, have generated recombinant domain-deleted antibodies. One example is the anti–carcinoembryonic antigen (CEA) T84.66 minibody, a dimeric engineered antibody fragment assembled $V_L$-linker-$V_H$-hinge-$C_H3$, where $V_L$ is the light chain variable region, $V_H$ is the heavy chain variable region, and $C_H3$ is the human IgG1 third constant domain (Fig. 1*A*). *In vivo*, the anti-CEA minibody displayed faster clearance kinetics, more rapid tumor targeting, and lowered normal organ metabolic uptake compared with the parental T84.66 antibody (1–3). Another domain-deleted recombinant antibody fragment, specifically discussed in this work, is the single-chain Fv-Fc (scFv-Fc), where the anti-CEA scFv ($V_L$-linker-$V_H$) fragment was joined to the intact Fc region ($C_H2$ and $C_H3$ domains) of human IgG1 via a hinge region [$(scFv\text{-}Fc)_2$, 105 kDa; Fig. 1*A*]. This antibody fragment, in contrast to the minibody, behaves similarly to intact antibodies specifically regarding serum persistence and tumor uptake (4, 5). The scFv-Fc antibody fragment includes an intact Fc region, which is crucial for prolonging the half-life of antibodies (6) and antibody fragments. Specific interactions between antibody Fc domain amino acid residues and the protective neonatal Fc receptor (FcRn; Brambell receptor) essentially divert IgGs from the lysosomal degradative pathway compared with other serum proteins (7–10).

The FcRn has long been known to control the transfer of immunity (IgGs) from the mother to the offspring (11–17). Recent studies have shown a more intricate function of the FcRn receptor in maintaining the levels of IgGs in the circulation (i.e., by favoring antibody recycling rather than catabolism; refs. 8–10). In vascular endothelial cells, IgGs are taken up from the serum by fluid-phase endocytosis and delivered to early endosomes where FcRn resides. IgG binds FcRn with high affinity at slightly acidic pH (<6.5) but with low affinity at neutral pH (18, 19). At modest levels of

**Request for reprints:** Anna M. Wu, Crump Institute for Molecular Imaging, Department of Molecular and Medical Pharmacology, David Geffen School of Medicine at University of California, Los Angeles, 700 Westwood Plaza, Los Angeles, CA 90095. Phone: 310-794-5088; Fax: 310-206-8975; E-mail: awu@mednet.ucla.edu.

antibody (due to the saturable nature of the intracellular FcRn-IgG interaction; ref. 20), most of the ligand binds FcRn and it is either recycled back to the circulation or delivered by transcytosis from the apical to the basolateral side of the endothelial cell. In either case, the neutral pH of the serum or the interstitial fluid promotes dissociation from the FcRn receptor and release of immunoglobulins. Essential for the FcRn binding, in both humans and rodents, are the residues $Ile^{253}$ and $His^{310}$ in the $C_H2$ domain and $His^{435}$ in the $C_H3$ domain (Kabat numbering system; Fig. 1*B*; refs. 21–24). Ward et al. showed that mutation of these amino acid residues correlates with reduced antibody fragment half-life (22). Furthermore, the solution of the structure of co-crystallized FcRn and Fc supported these findings by delineating the protein interface in human FcRn-human Fc and rat FcRn-rat Fc complexes (25, 26). Mutation of residues near the FcRn binding site can also result in prolonging antibody serum half-life. This approach involves enhancing the antibody affinity for binding to FcRn and can ultimately find clinical utility by increasing the serum persistence of therapeutic antibodies (27, 28).

Taking these findings into consideration, we decided to use the scFv-Fc fragment format (Fig. 1*C*), which shows pharmacokinetic similarity to the intact antibody, to generate variants that have the same molecular weight but exhibit a range of persistence in the circulation. To accomplish this goal, we engineered four T84.66 anti-CEA scFv-Fc single mutants (H435R, H435Q, H310A, and I253A) and one double mutant (H310A/H435Q) along with the wild-type (nonmutated) scFv-Fc. We designed these scFv-Fcs as chimeras composed of a human IgG1 Fc region with murine T84.66 $V_L$ and $V_H$ domains (Fig. 1*C*).

Following the *in vitro* biochemical characterization of each scFv-Fc recombinant protein, biodistribution studies were conducted in non-tumor-bearing mice to establish the serum clearance kinetic profiles of radio-iodinated scFv-Fc antibody fragments as well as the distribution of activity in other organs. To evaluate the tumor targeting potential of scFv-Fc antibody fragments in live mice, small animal positron emission tomography (PET) imaging was employed. In these studies, mice carrying CEA-positive xenografts were given $^{124}$I-labeled scFv-Fc fragments and imaged at different time points.

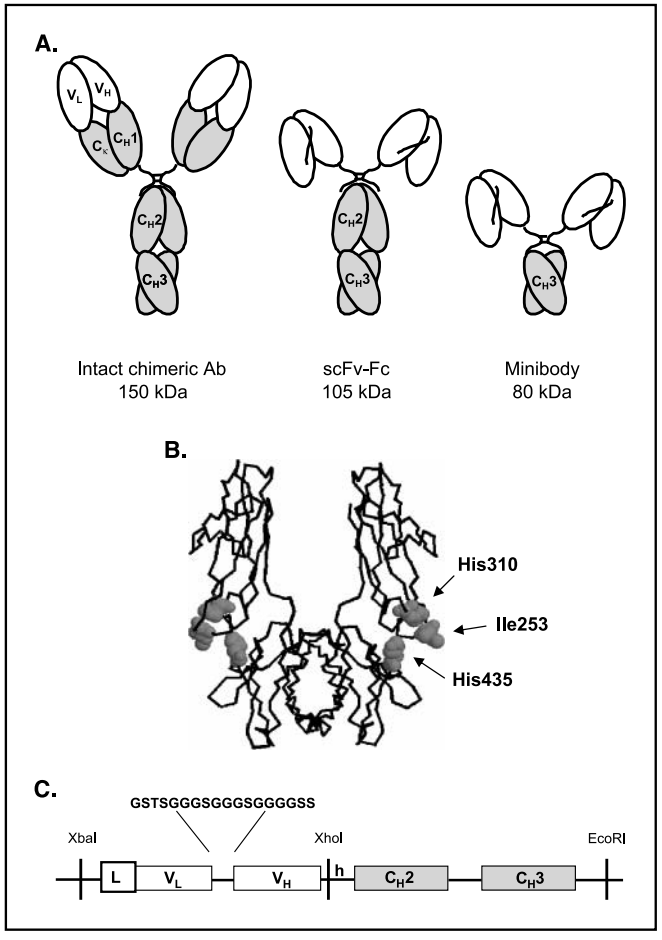


**Figure 1.** *A,* schematic representation of an intact chimeric antibody and engineered fragments. *B,* structure of the Fc region of human IgG1 with residues selected for mutation. The figure was generated using the RASMOL program (Roger Sayle, Bioinformatics Research Institute, University of Edinburgh, GB). *C,* design of the anti-CEA scFv-Fc fragment. Gene assembly including the 18 amino acid linker sequence between the V regions and the restriction sites used in the cloning and subcloning steps.

## Materials and Methods

**Design, Plasmids, and Gene Assembly.** The anti-CEA T84.66/GS18 scFv was composed of the murine $V_L$ and the murine $V_H$ linked through a glycine-serine–rich, 18–amino acid peptide (2). The scFv was then fused to the hinge, $C_H2$, and $C_H3$ domains of the human IgGγ1 to produce the scFv-Fc fragment (Fig. 1*C*).

The T84.66 scFv-Fc (~1,500 bp) was assembled in pUC18 plasmid (New England Biolabs, Beverly, MA) containing the native mammalian signal sequence. The entire scFv-Fc was excised from the pUC18 vector and ligated into the pEE12 mammalian expression vector (Lonza Biologics, Slough, United Kingdom) incorporating the glutamine synthetase gene (29). The scFv-Fc variants were generated at the pUC18 subcloning stage. Specific mutations were introduced in the $C_H2$ and $C_H3$ domains using a Quick-Change Site Directed Mutagenesis kit (Stratagene, La Jolla, CA) according to manufacturer's directions. The plus strand primers were H435R: 5′-GAGGCTCTGCACAACAGGTACACGCAGAAG-3′, H435Q: 5′-GAGGCTCTGCACAACCAGTACACGCAGAAG-3′, I253A: 5′-ACCCAAGGACACCCTCATGGCCTCCCGGACCCCTGAG-3′, and H310A: 5′-GTCCTCACCGTCCTGGCCCAGGACTGGTTGAATG-3′. For the generation of the H310A/H435Q double mutant, scFv-Fc H435Q template DNA was used with the H310A mutagenesis primers.

**Expression, Selection, and Purification.** NS0 murine myeloma cells ($1 \times 10^7$; ref. 30) were transfected with the pEE12 scFv-Fc constructs (linearized by digestion with *Sal*I) and subjected to selection in glutamine-deficient DMEM/high modified medium (JRH Biosciences, Lenexa, KS) as described (31). Antibody production was assayed by ELISA and evaluated by Western blot to coregister the antibody fragment expression with the expected molecular weight using the alkaline phosphatase–conjugated goat anti-human IgG, Fcγ specific. Selected clones were expanded into triple flasks (Nunclon, Rochester, NY). Harvested supernatants were centrifuged to remove cell debris and were treated with 5% (v/v) of a 50% (v/v) slurry of AG1-X8 resin (Bio-Rad Laboratories, Hercules, CA) in PBS to remove phenol red (31). The solution was filtered and dialyzed against 50 mmol/L Tris-HCl (pH 7.4) and then purified using AKTA Purifier (Amersham Biosciences AB, Uppsala, Sweden). Anion exchange chromatography using a 15 mL Source HQ50 column (Amersham Biosciences), pre-equilibrated with 50 mmol/L HEPES (pH 7.4), was used for the first step of purification. Bound proteins were eluted using a linear NaCl gradient from 0 to 0.2 mol/L in the presence of 50 mmol/L HEPES (pH 7.4). Fractions containing the protein of interest were analyzed by SDS-PAGE, pooled, and loaded onto a pre-equilibrated 8 mL ceramic hydroxyapatite column (Bio-Rad Laboratories). Bound proteins were eluted using a linear $K_3PO_4$ gradient from 0 to 0.06 mol/L in the presence of 50 mmol/L MES (pH 6.5). The final purification step consisted of an anion exchange chromatography using a 1 mL Source 15Q column (Amersham

Biosciences) under the same elution conditions as the first step of purification. Fractions containing the pure protein were pooled, dialyzed against PBS, and concentrated by Centriprep 30 (Millipore Corp., Bedford, MA). The final concentration of each purified protein was determined by $A_{280\ nm}$ using an extinction coefficient of $\varepsilon = 1.4$.

**Characterization of Purified scFv-Fc Fragments.** Purified proteins were analyzed by SDS-PAGE under reducing (1 mmol/L DTT) and nonreducing conditions. Purified fragments were also subjected to size exclusion chromatography on a Superdex 200 HR 10/30 column (Amersham Biosciences) run isocratically in 50 mmol/L $Na_3PO_4$, 0.15 mol/L NaCl (pH 7.0) buffer. A 0.1 mL volume containing 50 μg of pure protein was loaded onto the column and eluted at 0.5 mL/min flow rate. The CEA binding activity of scFv-Fc proteins was determined by competition ELISA as described (32). The normalized data were then used to calculate the relative binding affinities of each scFv-Fc fragment compared with the parental cT84.66 intact antibody.

**Radioiodination of scFv-Fc Fragments.** For biodistribution studies, radioiodination of the scFv-Fc fragments was done by the Iodo-Gen method as described (33). Briefly, ~0.2 mg of purified protein was labeled with either 0.2 mCi $Na^{125}I$ or $Na^{131}I$ (PerkinElmer Life Sciences, Inc., Boston, MA) in 0.1 mL phosphate buffer (pH 7.5) using polypropylene tubes coated with 20 μg Iodo-Gen (Pierce, Rockford, IL) for 5 to 7 minutes at room temperature. The sample was purified by a Gilson high-performance liquid chromatography (HPLC) system on a Superdex 75 column (Amersham Biosciences). The fractions containing the radioactive peak were selected and diluted in normal saline/1% human serum albumin to prepare doses for injection. The radiolabeling efficiency was determined by integrating areas on the size exclusion HPLC trace and calculating the percentage of radioactivity associated with the 105 kDa peak of the scFv-Fc. Immunoreactivity and valency were determined by incubation of the labeled protein with a 20-fold excess (w/w) of recombinant CEA in 0.15 mL PBS/1% human serum albumin. Analysis by size exclusion HPLC was done on Superose 6 HR 10/30 columns (Amersham Biosciences) to assess the formation of antibody-antigen complexes. Radioiodination with $^{124}I$ for the small animal PET studies was also accomplished by the Iodo-Gen method. Labeling reactions (0.1-0.2 mL) typically contained 0.1 to 0.2 mg purified protein and 0.5 to 1 mCi $Na^{124}I$ (Advanced Nuclide Technology, Indianapolis, IN). The labeling efficiency was measured by instant TLC using the Tec-Control kit (Biodex Medical Systems, Shirley, NY).

**Pharmacokinetic and Biodistribution Studies.** All animal studies were conducted under protocols approved by the City of Hope Research Animal Care Committee or the Chancellor's Animal Research Committee at University of California Los Angeles. Forty 7- to 8-week-old female BALB/c mice (The Jackson Laboratory, Bar Harbor, ME) were injected via the tail vein with a mixture of paired $^{125}I$- and $^{131}I$-labeled scFv-Fc antibody proteins in a single experiment. The wild-type, H435R, and H310A were labeled with $^{125}I$. For these three constructs, the protein doses per animal ranged from 2.4 to 4.5 μg and injected activity per mouse ranged from 3 to 10 μCi. The H435Q, I253A, and H310A/H435Q proteins were labeled with $^{131}I$. The protein doses per animal ranged from 1.8 to 3.7 μg and injected activity was from 1 to 2.5 μCi per mouse. For the three dual biodistributions, we made the following pairs: H435Q with H435R, H310A with H310A/H435Q, and I253A with the wild-type scFv-Fc. At 0, 2, 4, 6, 12, 24, 48, and 72 hours post injection, groups of five mice were euthanized and dissected; major organs were weighed and counted in a gamma scintillation counter (Wizard 3, PerkinElmer Life Sciences). $^{125}I$ emission was read at a window of 15 to 70 keV, whereas the $^{131}I$ gamma counter reading window was 260 to 430 keV. Activities in liver, spleen, kidney, lung, bone, carcass, and blood were determined; background, crossover, and decay corrected; and converted to percentage injected dose per gram (%ID/g). To quantitate the differences in blood clearance profiles, the ADAPTII software package (34) was used to estimate two rate constants characteristic of each engineered fragment. A bi-exponential function was fitted, via the ID subroutine, to each blood clearance curve (%ID/g). Significant differences in these values were examined by comparing the 95% confidence intervals for the estimated parameters.

**Xenograft Imaging.** The imaging experiments used the P4 and Focus microPET (Concorde Microsystems, Inc., Knoxville, TN) instruments. For the studies, 7- to 8-week-old athymic mice (Charles River Laboratories, Wilmington, MA) were injected s.c. in the left shoulder region with $1 \times 10^6$ to $5 \times 10^6$ LS174T human colon carcinoma cells (American Type Culture Collection, Manassas, VA) and the right shoulder with approximately the same number of C6 glioma cells (American Type Culture Collection). Tumor masses were allowed to develop for ~10 days and reached ~100 to 200 mg weight. Before conducting imaging studies, thyroid uptake of radioiodine was blocked by pretreatment of the mice with 10 drops of saturated potassium iodide/100 mL drinking water for 24 hours. Stomach uptake was blocked by administration of 1.5 mg potassium perchlorate in 0.2 mL PBS by gastric lavage 30 minutes before injection. Mice were injected in the tail vein with ~0.1 mCi $^{124}I$-labeled scFv-Fc in saline/1% human serum albumin. At three different time points, mice were anesthetized using 2% isoflurane, placed on the microPET bed, and imaged. Acquisition time was 10 minutes. Mice injected with $^{124}I$-labeled scFv-Fc H435Q, I253A, and H310A/H435Q proteins were imaged by the P4 small animal PET imaging system. The $^{124}I$-labeled scFv-Fc wild-type and H310A injected animals were imaged via the Focus microPET instrument. All images were reconstructed using a FBP algorithm (35) and displayed by the AMIDE software package (36). The same color threshold was applied to all images. Regions of interest were drawn for the LS174T CEA-positive tumors centered on the area with highest activity. A low-activity, soft-tissue region in the lower body and an area of increased background activity in the abdominal region were also part of the region of interest analysis. Approximately equal-sized regions of interest were drawn. Tumor-to-background and tumor-to-soft tissue ratios were determined for individual mice and averaged for each time point and construct. Following the last scanning time point, animals were euthanized, tumors excised, weighed, and counted in a well counter (Cobra II Auto-Gamma, Packard, IL), and after decay correction, the %ID/g was calculated.

**Statistical Analysis.** To compare differences in average %ID/g over time among the different constructs, two-way ANOVA was done. Time (hours), scFv-Fc group, and the interaction between these two factors were used to predict %ID/g within each organ for each of 15 pairings of constructs. In addition, the *t* test was employed to compare %ID/g between the constructs at specific times (24 and 48 hours). All significance testing was done at the $P < 0.01$ level. Tukey test was used for multiple comparisons in blood and organs and for the separation of means in significant groups. The SAS/STAT software (SAS, Inc., Cary, NC) was used for all statistical models and analyses. From the microPET images, the comparisons of tumor-to-background and tumor-to-soft tissue ratios among constructs employed the unpaired *t* test using Prism software (GraphPad Software for Science, San Diego, CA).

## Results

**Expression and Purification.** All six T84.66 scFv-Fc fragments were expressed in NS0 mouse myeloma cells using the glutamine synthetase expression/selection system (29). Cell clones expressing the highest levels of scFv-Fc in culture supernatants as determined by ELISA were selected for expansion. The expression level of the selected scFv-Fc clones ranged from 15 to 40 μg/mL in T-flasks. An initial attempt was made to purify the scFv-Fcs in one step by protein A affinity chromatography. This was feasible for the isolation of all scFv-Fcs, except the H310A/H435Q double mutant [most likely because the FcRn binding region overlaps with protein A interactions (37)]. For purposes of consistency, ion exchange chromatography was selected, as it is not affected by the Fc mutations and the same elution profile could be applied to all six constructs. The theoretical isoelectric point of the fragments was calculated and ranged from 5.8 for the double mutant to 6.0 for

the H435Q, suggesting the use of an anion exchange column. To achieve higher purity, ceramic hydroxyapatite chromatography and a second round of anion exchange chromatography were incorporated in the purification strategy. The use of this three-step purification scheme allowed for the production of homogeneous preparations of scFv-Fc recombinant fragments with ~98% purity (calculated by integration of protein peaks on size exclusion chromatography profiles). A volume of ~300 mL culture supernatant containing each scFv-Fc fragment was purified and yielded 3.1 to 11.6 mg of pure protein.

**Biochemical Characterization of scFv-Fc Proteins.** SDS-PAGE under both nonreducing and reducing conditions was used to confirm the purity of each construct (Fig. 2*A*). *Lanes 1*, *2*, and *3* and *4*, *5*, and *6* correspond to scFv-Fc H435Q, wild-type and H310A fragments under nonreducing and reducing conditions, respectively. *Lanes 7*, *8*, and *9* and *10*, *11*, and *12* represent scFv-Fc H310A/H435Q, I253A, and H435R constructs under nonreducing and reducing conditions, respectively. The migration of the scFv-Fc was consistent with the calculated molecular weight of ~105 kDa. Under reducing conditions, the expected scFv-Fc monomers of ~53 kDa were observed. A Western blot (data not shown) using alkaline phosphatase–conjugated goat anti-human Fc-specific IgG and alkaline phosphatase–conjugated goat anti-mouse $F(ab')_2$-specific IgG confirmed that the additional bands on the SDS-PAGE gel under reducing conditions were cleavage products of the scFv-Fc and not impurities.

Size exclusion chromatography was done to evaluate the native state of scFv-Fc variant proteins (Fig. 2*B*). The chromatograms show that each fragment eluted as a single peak with elution time consistent with the rest of the scFv-Fcs ranging from 27.2 to 27.5 minutes. Furthermore, the elution time of all scFv-Fc antibody fragments was intermediate between the elution times of the intact antibody (25.78 minutes, 150 kDa) and the minibody (28.45 minutes, 80 kDa), whereas the diabody eluted much later (38.16 minutes, 55 kDa) due to its smaller molecular weight. This confirmed that the size of the fragments is between that of the intact IgG1 and the minibody, consistent with the expected value of 105 kDa.

**Functional Characterization of the scFv-Fc Proteins.** Competition ELISA showed the ability of the purified scFv-Fcs to bind the recombinant N-A3 antigen. Three fragments (scFv-Fc wild-type, I253A, and H310A/H435Q) were selected and compared with the parental cT84.66 antibody in their ability to compete for binding to the antigen epitope. Fifty percent displacement occurred at ~1.9, 2.5, and 2.7 nmol/L of the unlabeled scFv-Fc H310A/H435Q, I253A, and wild-type, respectively (Fig. 3). Thus, the relative binding affinity of scFv-Fcs ranged from $1.9 \times 10^9$ to $2.7 \times 10^9$ mol/L$^{-1}$ compared with $1.1 \times 10^9$ mol/L$^{-1}$ for the parental cT84.66 antibody.



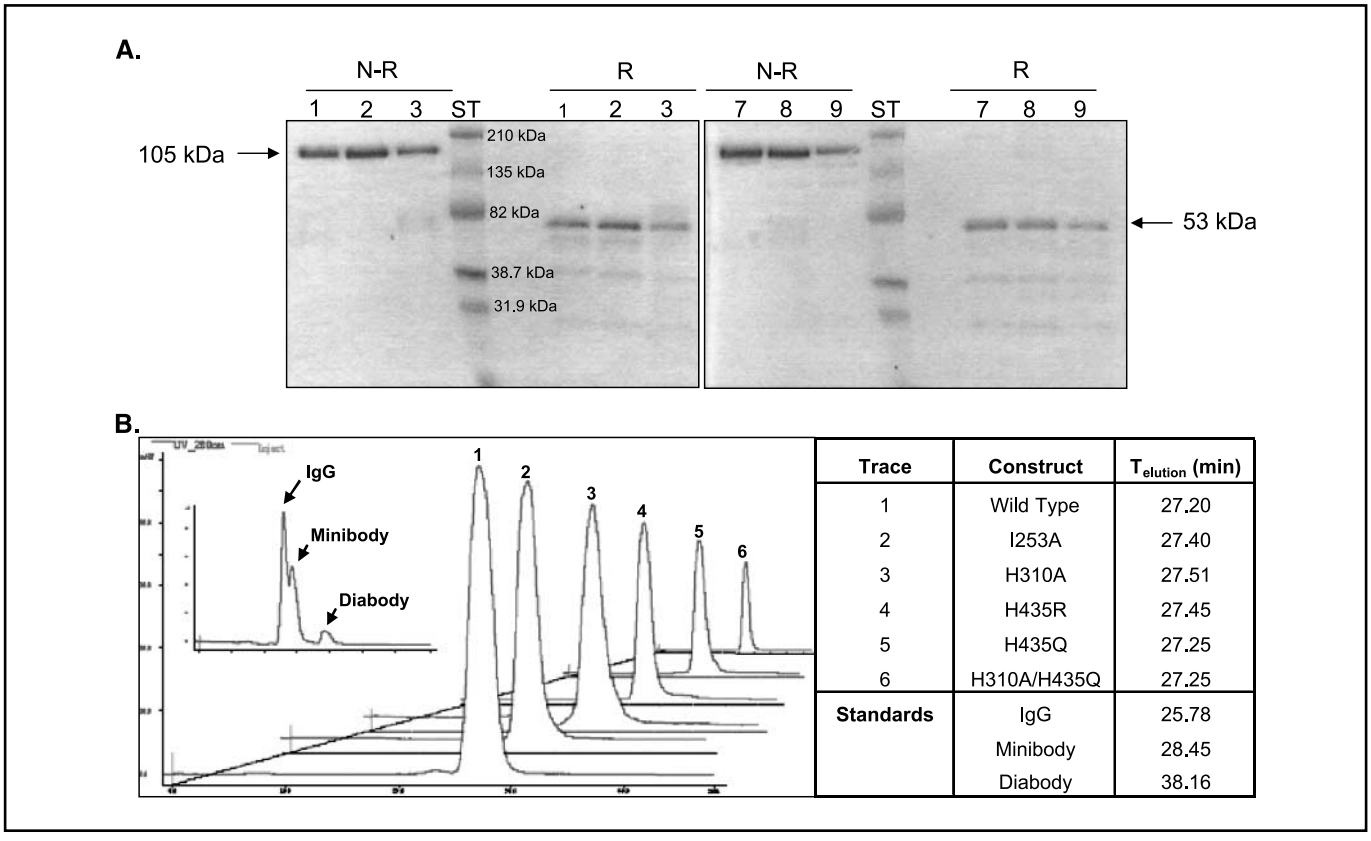


| Trace | Construct | $T_{elution}$ (min) |
|---|---|---|
| 1 | Wild Type | 27.20 |
| 2 | I253A | 27.40 |
| 3 | H310A | 27.51 |
| 4 | H435R | 27.45 |
| 5 | H435Q | 27.25 |
| 6 | H310A/H435Q | 27.25 |
| **Standards** | IgG | 25.78 |
| | Minibody | 28.45 |
| | Diabody | 38.16 |

**Figure 2.** *A,* SDS-PAGE. *Lanes 1*, *2*, and *3,* nonreduced (*N-R*) H435Q, wild-type, and H310A, respectively; *lanes 4*, *5*, and *6,* reduced (*R*) H435Q, wild-type, and H310A, respectively; *lanes 7*, *8*, and *9,* nonreduced H310A/H435Q, I253A, and H435R, respectively; *lanes 10*, *11*, and *12*, reduced H310A/H435Q, I253A, and H435R, respectively. *B,* size exclusion chromatography. Experiments were done using a Superdex 200 HR 10/30 column. Intact cT84.66 IgG1 (150 kDa; ref. 45), minibody [$(scFv\text{-}C_H3)_2$, 80 kDa; ref. 1], and diabody [$(scFv)_2$, 55 kDa; ref. 33] were used as size standards.

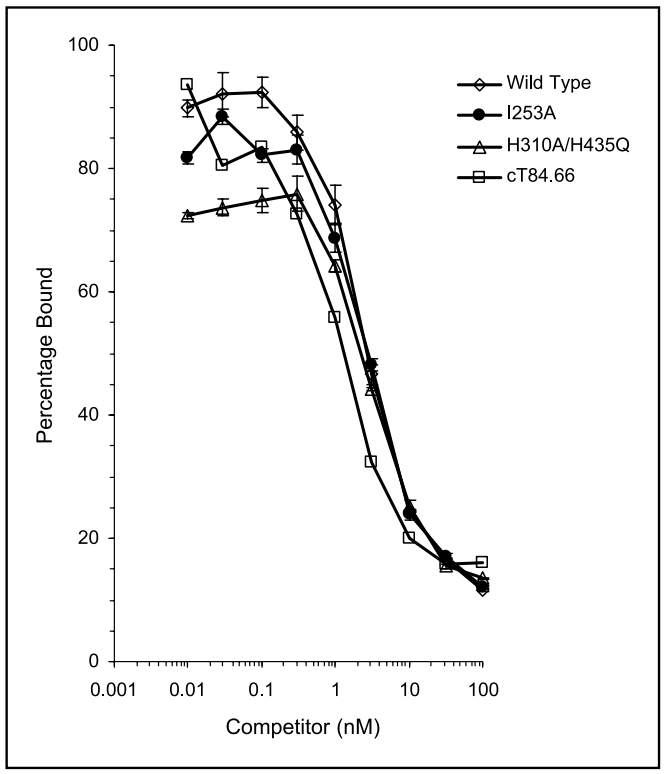


**Figure 3.** Competition ELISA binding assay. Plates were coated with recombinant NA-3 antigen. Increasing concentrations of wild-type, I253A, and H310A/H435Q unlabeled fragments were used to compete out the biotinylated intact, cT84.66 anti-CEA monoclonal antibody.

The immunoreactivity of scFv-Fcs was also analyzed following the radioiodination step by solution-phase incubation in the presence of a 20-fold excess of CEA. Size exclusion HPLC analysis showed that 90% to 95% of the radiolabeled scFv-Fcs were shifted to higher molecular weight complexes following the incubation with CEA (data not shown).

**Murine Biodistribution Studies.** Dual-label biodistribution and clearance studies of $^{125}$I- and $^{131}$I-radiolabeled scFv-Fcs were conducted in BALB/c mice. The labeling efficiency for the scFv-Fc proteins ranged from 85% to 99.5%, with the exception of the scFv-Fc H310A variant, for which labeling efficiency was 27%. The immunoreactivity of all but the H310A fragment ranged from 85% to 98%, whereas H310A was 70%. The scFv-Fc order of serum clearance from the slowest to the fastest clearing fragment was as follows: wild-type > H435R > H435Q > I253A > H310A > H310A/H435Q (Fig. 4). There was >50-fold difference in remaining blood activity at 72 hours post injection between wild-type and double mutant scFv-Fc antibody fragments (Table 1; $P < 0.0001$). Activities in all other organs were significantly lower than that in blood, with lung being the organ with the next highest %ID/g. The ANOVA analysis across the entire blood curves from Table 1 confirmed that the main effect of each construct was statistically different from that of any other scFv-Fc, with the exception of the H435R comparison with H435Q ($P = 0.047$). Thus, five of six scFv-Fc constructs exhibited statistically distinguishable serum clearance kinetics. The Tukey test, employing multiple comparisons of the overall organ/blood means of scFv-Fc fragments, allowed for separation of the constructs in significantly different groups. Whether constructs formed their own, statistically distinct groups (in bone and in lung) or paired in the same group (in blood: H435R and H435Q, in liver: I253A and H310A, in kidney: wild-type and H435R; I253A and H310A, in spleen: wild-type and H435R, and in carcass: H435R and H435Q; I253A and H310A), the group order remained the same: wild-type followed by H435R, H435Q, I253A, H310A, and H310A/H435Q mutant. The order of uptake was also consistent in nearly all organs and in blood at 24 and 48 hours, which multiple comparisons using Tukey groupings further confirmed. Data from Table 1 were used to calculate the half-lives of scFv-Fc fragments. As shown in Table 2, the scFv-Fc recombinant antibody fragments exhibited a wide spectrum of terminal half-lives ($t_{1/2\beta}$) ranging from ~12 days (wild-type) to 8 hours (H310A/H435Q), whereas the $t_{1/2\alpha}$ for the mutant proteins were less variable. The blood activity that cleared with both rapid and slow kinetics was also similar for all six constructs and averaged $A_\alpha$ of 51% and $A_\beta$ of 49%. In addition to the distribution-phase half-life ($t_{1/2\alpha}$) ($t_{1/2\alpha}$) and the terminal elimination phase half-life ($t_{1/2\beta}$) of each fragment, the mean residence time was calculated as a single variable for blood clearance (38). The mean residence time of the scFv-Fc fragments ranged from 17.1 days (wild-type) to 10.7 hours (H310A/H435Q). Area under the curve was also computed for each construct (%ID/g × hours).

**Xenograft Imaging Studies.** MicroPET imaging was employed to evaluate the *in vivo* tumor targeting ability of the recombinant scFv-Fc constructs. For this purpose, athymic mice carrying CEA-positive (LS174T colorectal carcinoma) and CEA-negative control (C6 glioma) tumors were injected with $^{124}$I-labeled scFv-Fcs. The $^{124}$I labeling efficiency ranged from 65% to 98.8%. MicroPET imaging studies were conducted in four animals per construct, bearing CEA-positive tumors averaging 110 mg

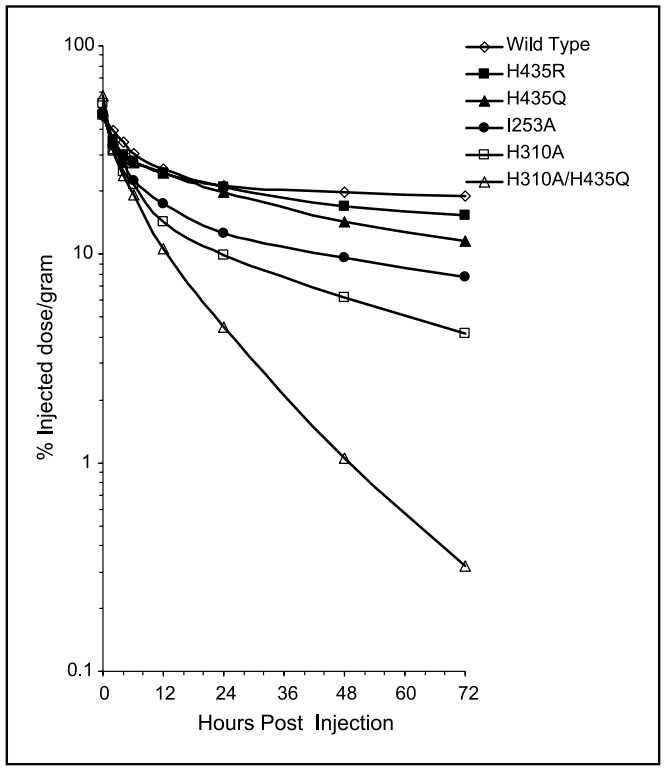


**Figure 4.** Blood activity curves. Dual biodistribution studies with $^{125}$I- and $^{131}$I-labeled scFv-Fcs (Table 1).

**Table 1.** Biodistribution of $^{125}$I and $^{131}$I-labled T84.66 scFv-Fc fragments in BALB/c mice

| Organ (%ID/g) | 0 | 2 | 4 | 6 | 12 | 24 | 48 | 72 |
|---|---|---|---|---|---|---|---|---|
| $^{125}$I-scFv-Fc wild-type | | | | | | | | |
| **Blood** | **45.7** (2.86) | **39.2** (1.17) | **34.4** (1.21) | **30.3** (0.61) | **25.6** (0.70) | **21.4** (0.76) | **19.9** (1.17) | **19.0** (0.54) |
| Liver | 10.7 (0.78) | 9.16 (0.24) | 8.31 (0.14) | 7.28 (0.36) | 5.43 (0.18) | 5.52 (0.35) | 4.72 (0.15) | 4.57 (0.27) |
| Spleen | 16.3 (1.42) | 13.3 (0.39) | 10.9 (0.34) | 9.90 (1.00) | 6.98 (0.35) | 6.49 (0.27) | 5.89 (0.46) | 6.18 (0.35) |
| Kidney | 10.7 (0.95) | 9.65 (0.90) | 8.89 (0.76) | 7.82 (0.49) | 7.58 (0.23) | 5.89 (0.25) | 5.99 (0.32) | 5.86 (0.23) |
| Lung | 15.3 (1.58) | 13.8 (0.52) | 13.2 (0.44) | 13.0 (0.61) | 10.8 (0.66) | 8.84 (0.36) | 9.22 (0.30) | 9.49 (0.35) |
| Bone | 4.19 (0.39) | 4.84 (0.33) | 3.90 (0.14) | 3.90 (0.15) | 3.29 (0.18) | 2.93 (0.09) | 2.69 (0.27) | 2.64 (0.13) |
| Carcass | 1.94 (0.13) | 2.44 (0.07) | 2.52 (0.06) | 2.50 (0.04) | 2.62 (0.04) | 2.63 (0.10) | 2.41 (0.06) | 2.68 (0.06) |
| $^{125}$I-scFv-Fc H435R | | | | | | | | |
| **Blood** | **46.3** (1.38) | **35.1** (2.41) | **29.9** (0.73) | **28.1** (0.67) | **24.7** (0.98) | **21.1** (0.49) | **17.1** (0.42) | **15.4** (0.24) |
| Liver | 12.8 (0.29) | 10.3 (0.56) | 9.27 (0.36) | 8.80 (0.22) | 6.06 (0.34) | 5.43 (0.35) | 4.22 (0.12) | 3.86 (0.20) |
| Spleen | 16.8 (0.66) | 13.3 (1.06) | 11.5 (0.62) | 10.1 (0.56) | 8.01 (0.37) | 7.05 (0.46) | 5.45 (0.34) | 4.86 (0.24) |
| Kidney | 12.3 (0.52) | 10.8 (0.67) | 9.49 (0.40) | 8.66 (0.59) | 7.17 (0.50) | 5.76 (0.30) | 4.51 (0.23) | 3.90 (0.24) |
| Lung | 14.1 (0.80) | 13.6 (1.24) | 11.5 (0.59) | 11.4 (0.43) | 10.6 (0.66) | 8.74 (0.27) | 7.43 (0.17) | 6.58 (0.24) |
| Bone | 4.39 (0.45) | 4.34 (0.32) | 3.88 (0.31) | 3.21 (0.17) | 3.35 (0.19) | 2.87 (0.12) | 2.25 (0.05) | 2.11 (0.14) |
| Carcass | 1.69 (0.12) | 2.32 (0.08) | 2.37 (0.08) | 2.39 (0.06) | 2.55 (0.07) | 2.42 (0.06) | 2.23 (0.05) | 2.03 (0.07) |
| $^{131}$I-scFv-Fc H435Q | | | | | | | | |
| **Blood** | **48.9** (1.20) | **35.6** (2.49) | **30.0** (0.81) | **27.4** (0.66) | **24.5** (0.98) | **19.7** (0.43) | **14.3** (0.43) | **11.5** (0.21) |
| Liver | 9.46 (0.47) | 7.41 (0.43) | 6.85 (0.20) | 6.56 (0.23) | 5.06 (0.29) | 4.05 (0.22) | 2.90 (0.12) | 2.34 (0.12) |
| Spleen | 12.2 (0.44) | 9.06 (0.82) | 8.68 (0.39) | 7.67 (0.51) | 6.40 (0.33) | 5.64 (0.40) | 3.98 (0.30) | 3.17 (0.17) |
| Kidney | 12.0 (0.44) | 9.56 (0.64) | 8.70 (0.43) | 7.77 (0.57) | 6.69 (0.49) | 5.07 (0.30) | 3.53 (0.19) | 2.74 (0.18) |
| Lung | 14.0 (0.81) | 12.7 (1.20) | 10.8 (0.53) | 10.3 (0.45) | 9.89 (0.64) | 7.84 (0.28) | 5.65 (0.15) | 4.55 (0.19) |
| Bone | 4.08 (0.37) | 3.87 (0.29) | 3.51 (0.24) | 2.85 (0.15) | 3.17 (0.19) | 2.60 (0.13) | 1.81 (0.05) | 1.51 (0.09) |
| Carcass | 1.84 (0.12) | 2.44 (0.07) | 2.50 (0.09) | 2.49 (0.07) | 2.59 (0.08) | 2.40 (0.07) | 1.94 (0.05) | 1.61 (0.06) |
| $^{131}$I-scFv-Fc I253A | | | | | | | | |
| **Blood** | **48.1** (3.17) | **33.1** (0.97) | **27.1** (1.06) | **2.5** (0.54) | **17.4** (0.46) | **12.7** (0.44) | **9.58** (0.63) | **7.76** (0.22) |
| Liver | 11.1 (0.73) | 7.47 (0.14) | 6.17 (0.17) | 5.15 (0.26) | 3.55 (0.09) | 3.11 (0.16) | 2.14 (0.10) | 1.81 (0.10) |
| Spleen | 13.9 (1.17) | 9.64 (0.22) | 7.78 (0.31) | 6.60 (0.60) | 4.25 (0.20) | 3.58 (0.15) | 2.58 (0.19) | 2.35 (0.13) |
| Kidney | 11.2 (0.91) | 7.98 (0.65) | 6.79 (0.59) | 5.70 (0.37) | 4.96 (0.18) | 3.46 (0.14) | 2.79 (0.18) | 2.39 (0.10) |
| Lung | 14.7 (1.53) | 11.5 (0.39) | 10.2 (0.39) | 9.38 (0.44) | 7.03 (0.43) | 5.16 (0.21) | 4.11 (0.16) | 3.64 (0.15) |
| Bone | 3.92 (0.37) | 3.95 (0.25) | 3.05 (0.15) | 2.85 (0.09) | 2.17 (0.13) | 1.72 (0.05) | 1.27 (0.14) | 1.14 (0.07) |
| Carcass | 2.02 (0.17) | 2.53 (0.07) | 2.41 (0.10) | 2.17 (0.04) | 2.01 (0.03) | 1.87 (0.08) | 1.35 (0.05) | 1.39 (0.04) |
| $^{125}$I-scFv-Fc H310A | | | | | | | | |
| **Blood** | **53.2** (2.08) | **31.1** (0.57) | **5.0** (0.74) | **21.6** (0.55) | **14.4** (0.52) | **9.85** (0.32) | **6.18** (0.19) | **4.15** (0.26) |
| Liver | 16.8 (0.58) | 7.90 (0.11) | 6.88 (0.22) | 6.23 (0.41) | 3.61 (0.07) | 2.52 (0.10) | 1.52 (0.05) | 1.15 (0.06) |
| Spleen | 13.5 (0.65) | 7.34 (0.16) | 7.18 (0.19) | 5.82 (0.50) | 3.75 (0.10) | 2.84 (0.18) | 1.71 (0.11) | 1.26 (0.09) |
| Kidney | 16.2 (0.52) | 8.63 (0.29) | 7.10 (0.41) | 6.53 (0.29) | 4.23 (0.08) | 2.86 (0.04) | 1.87 (0.07) | 1.32 (0.06) |
| Lung | 14.6 (0.79) | 11.8 (0.50) | 9.22 (0.28) | 8.40 (0.20) | 6.05 (0.29) | 4.13 (0.15) | 2.57 (0.06) | 1.82 (0.13) |
| Bone | 4.48 (0.18) | 3.52 (0.19) | 3.08 (0.22) | 2.59 (0.16) | 2.00 (0.10) | 1.33 (0.06) | 0.76 (0.03) | 0.64 (0.03) |
| Carcass | 2.50 (0.15) | 2.70 (0.12) | 2.73 (0.12) | 2.57 (0.17) | 2.02 (0.03) | 1.66 (0.05) | 1.21 (0.05) | 0.95 (0.03) |
| $^{131}$I-scFv-Fc H310A/H435Q | | | | | | | | |
| **Blood** | **57.4** (2.00) | **32.0** (0.64) | **24.0** (0.75) | **19.4** (0.50) | **0.7** (0.46) | **4.47** (0.18) | **1.06** (0.03) | **0.32** (0.03) |
| Liver | 13.5 (0.48) | 6.85 (0.07) | 5.41 (0.18) | 4.46 (0.33) | 2.18 (0.05) | 0.97 (0.04) | 0.33 (0.01) | 0.20 (0.01) |
| Spleen | 12.6 (0.63) | 6.88 (0.18) | 6.39 (0.11) | 4.95 (0.43) | 2.63 (0.07) | 1.25 (0.10) | 0.31 (0.02) | 0.10 (0.01) |
| Kidney | 12.6 (0.58) | 7.85 (0.29) | 6.18 (0.35) | 5.41 (0.27) | 2.94 (0.06) | 1.25 (0.04) | 0.35 (0.01) | 0.14 (0.01) |
| Lung | 14.2 (0.76) | 11.5 (0.53) | 8.67 (0.30) | 5.76 (1.46) | 4.56 (0.34) | 1.89 (0.07) | 0.48 (0.01) | 0.18 (0.02) |
| Bone | 4.28 (0.14) | 3.51 (0.18) | 3.02 (0.23) | 2.43 (0.22) | 1.59 (0.09) | 0.67 (0.05) | 0.19 (0.02) | 0.03 (0.01) |
| Carcass | 2.27 (0.16) | 2.57 (0.12) | 2.59 (0.13) | 2.33 (0.16) | 1.60 (0.05) | 0.94 (0.04) | 0.51 (0.05) | 0.35 (0.02) |

NOTE: Groups of five mice were analyzed at each time point. Organ uptake is expressed as %ID/g [mean (SE)].

(range, 28-216 mg). Whole body microPET scans were obtained at 4, 18, and 48 hours post injection (wild-type); 3, 18, and 90 hours (H435Q); 3, 18, and 48 hours (I253A); 4, 16, and 52 hours (H310A); and 4, 18, and 52 hours (H310A/H435Q). Figure 5 illustrates a representative member from each study. Tumor-to-background and tumor-to-soft tissue ratios were calculated for each animal and the averaged results were used for the generation of Fig. 6 (positive-to-control tumor ratios were not calculated because the control C6 tumors were not visible on any of the images). Comparison of tumor-to-nontarget ratios of fragment pairs at early, intermediate, and late time points was done. As expected, in the early time point, the tumor-to-background and tumor-to-soft tissue ratios achieved by the scFv-Fc proteins were essentially the same (Fig. 6). In the intermediate time point, the faster clearing constructs (H310A and H310A/H435Q) began to diverge from the slower ones

**Table 2.** Estimated values of blood half-times for the T84.66 cFv-Fcγ1 fragments

| Antibody fragment | $t_{½\alpha}$ (h) | $A_\alpha$* (%ID/g) | $t_{½\beta}$ (h) | $A_\beta$ (%ID/g) | Area under the curve† | Mean residence time (h)‡ |
|---|---|---|---|---|---|---|
| Wild-type | 4.22 | 23.3 | 289 | 22.4 | 9,480 | 411 |
| H435R | 1.87 | 19.5 | 83.4 | 26.6 | 3,250 | 118 |
| H435Q | 1.53 | 20.9 | 52.6 | 28.0 | 2,170 | 74 |
| I253A | 2.31 | 28.9 | 51.7 | 18.8 | 1,497 | 70 |
| H310A | 1.66 | 32.6 | 27.2 | 20.2 | 873 | 36 |
| H310A/H435Q | 0.86 | 25.2 | 8.00 | 32.3 | 402 | 11 |

*Amplitudes of the two components are given by $A_\alpha$ and $A_\beta$, where the sum of $A_\alpha$ and $A_\beta$ is the total %ID/g.
† Area under the curve is a time integral of the blood uptake (%ID/g × h).
‡ Mean residence time used to give a single variable for blood clearance.

(wild-type, H435Q, and I253A). During the late time point, when most of the activity in the nonspecific areas had cleared, all five fragments segregated from one another and achieved statistically distinct tumor-to-nontarget activities ($P < 0.01$). At the last time point, the H310A/H435Q mutant produced a 11.7:1 tumor-to-background ratio, whereas the H310A, I253A, H435Q, and wild-type scFv-Fc achieved 6.2:1, 1.8:1, 0.8:1, and 0.6:1, respectively (Fig. 6).

Following the last time point, mice were sacrificed and the dissected tumors were counted in a well counter. The tumor activities of the animals ($n = 4$) used in the microPET imaging studies were as follows: wild-type 41.9 ± 1.0% ID/g (tumor weight 142 ± 60 mg) at 48 hours post injection, H435Q 8.9 ± 1.2% ID/g (49 ± 10 mg) at 123 hours, I253A 12.0 ± 3.5% ID/g (94 ± 84 mg) at 50 hours, H310A 9.4 ± 2.1% ID/g (136 ± 57 mg) at 53 hours, and H310A/H435Q 5.3 ± 1.6% ID/g (130 ± 42 mg) at 55 hours. Overall, similar tumor sizes produced similar tumor uptake values within the same construct animal group. From the counting data, the positive (LS174T) to negative (C6) tumor uptake ratios were 5.3:1 (at 48 hours), 2.4:1 (at 123 hours), 3.6:1 (at 50 hours), and 6.5:1 (at 53 hours) for the wild-type, H435Q, I253A, and H310A constructs, respectively. The C6 tumor of the H310A/H435Q injected mice failed to grow.

## Discussion

The present study shows that the biological half-life of recombinant antibodies containing the Fc region can be readily manipulated by site-directed mutagenesis at sites where the Fc interacts with the protective FcRn receptor. Use of scFv-Fc format facilitated mutagenesis and expression of the wild-type and the five variants. Biochemical and biological characterization showed that all six proteins assembled into the expected 105 kDa fragments and bound antigen effectively. This allowed evaluation of the effect of FcRn interaction on the *in vivo* distribution and clearance properties of these otherwise identical engineered antibody fragments.

Dual biodistribution studies using $^{125}$I and $^{131}$I labels showed that each scFv-Fc recombinant antibody fragment possesses a distinct blood clearance rate, with scFv-Fc wild-type exhibiting the longest terminal serum half-life as expected (12 days). Among the mutants, scFv-Fc H435R persisted in circulation the longest, with a terminal half-life of 83.4 hours followed by the H435Q variant. The concept behind generating the H435R and H435Q mutants was to mimic the two protonation states of the His$^{435}$ residue under acidic (pH 6.5, optimal for FcRn binding) and neutral (pH 7.4, release from the FcRn) environments. At acidic pH, the His residue (imidazole side chain p$K_a$ is between 6 and 7) is protonated, thus positive in charge. This positively charged state is mimicked by the arginine residue (side chain p$K_a$ 12.5), promoting FcRn binding at both acidic and neutral pH of the endosomes and serum, respectively, and thus might interfere with release of the antibody fragment in the circulation. This may explain why the H435R variant has a longer half-life in comparison with the other mutants. On the other hand, the glutamine residue (polar and uncharged), substituting His$^{435}$ in the H435Q variant, remains neutral in both acidic and neutral environments. Thus, the half-life of this fragment is reduced more than the H435R construct. The hydrophobic Ile$^{253}$ residue is thought to be important for the proper packing of the Fc-FcRn heterodimer (26). The ablation of Ile$^{253}$ function by substitution with an alanine residue is possibly interfering with the proper FcRn-Fc association. This could explain why the I253A mutant clears faster than either H345Q or H435R fragments (24). His$^{435}$ and His$^{310}$ are clearly critical in providing antibody serum persistence, more so than other residues such as the Ile$^{253}$. In studies mapping the site on human IgG for binding of the FcRn receptor, Ward et al. showed that human Fc fragments with H435A and H310A mutations had lost >93% of their affinity for the recombinant soluble mouse FcRn receptor (22). In confirmation of these findings, our data showed that the H310A scFv-Fc variant is clearly compromised in its ability to remain in circulation. It is not surprising that when both histidine residues are mutated, in the H310A/H435Q double mutant construct, the serum clearance is accelerated the most.

The biodistribution data clearly show the ability to modulate the pharmacokinetics of a large antibody fragment, such as the scFv-Fc, by attenuating specific receptor interactions. Therefore, instead of producing one fragment with one distinct pharmacokinetic profile, we can produce several fragments with the same format exhibiting broadly different pharmacokinetic characteristics. Thus, one can choose a format that would best suit a specific *in vivo* application. A biodistribution study using $^{125}$I-labeled scFv-Fc wild-type in athymic nude mice bearing LS174T xenografts (data not shown) as well as direct counting of tumors from mice imaged using the wild-type scFv-Fc (see RESULTS) demonstrated that the overall tumor targeting ability of scFv-Fc wild-type is very similar to that of the $^{131}$I-labeled parental cT84.66 (39). Thus, if properties exhibited by intact antibodies are being sought, the scFv-Fc wild-type can be a comparable substitution. Alternatively, through the introduction of specific mutations, the same scFv-Fc fragment can be tailored to clear from the serum as quickly as a minibody.

The mouse FcRn receptor is promiscuous in its ability to bind human IgGs (40). This finding made it possible for us to study our chimeric scFv-Fc recombinants in the murine system and expect that the injected fragments will compete for the mouse FcRn receptor to a similar degree as the endogenous mouse IgGs. Moreover, the site of binding for rodent FcRn on human and

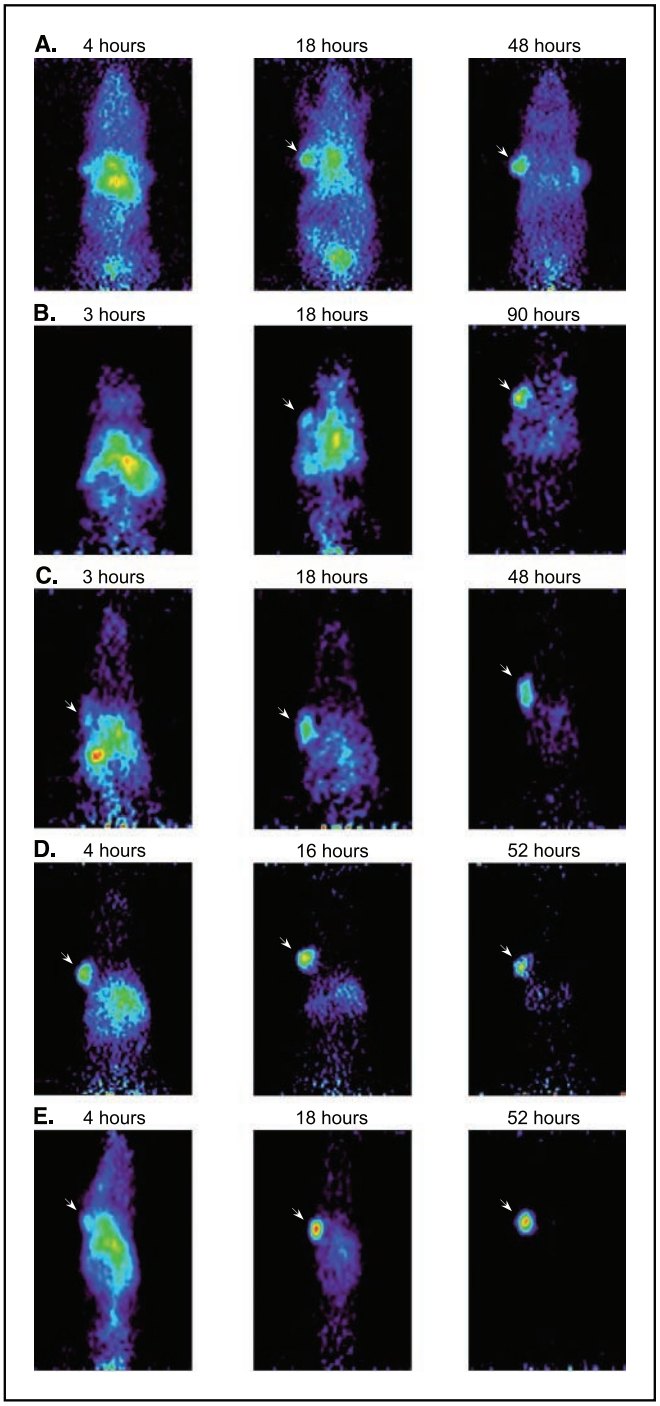


**Figure 5.** Coronal microPET images of five constructs in representative individual athymic mice bearing LS174T xenografts (left shoulder) and C6 (right shoulder, except *D*) at three different time points. *Arrow,* CEA-positive tumors. Following the imaging studies, tumors were dissected, weighed, and counted in a gamma counter. *A,* wild-type 42.5% ID/g, 185 mg LS174T tumor weight at 48 hours post injection; *B,* H435Q 10.6% ID/g, 64 mg at 123 hours; *C,* I253A 13.7% ID/g, 216 mg at 50 hours; *D,* H310A 10.6% ID/g, 174 mg at 53 hours; and *E,* H310A/H435Q 7.3% ID/g, 80 mg at 55 hours.

mouse IgG molecules closely overlaps and includes the $Ile^{253}$, $His^{310}$, and $His^{435}$ residues (21, 22, 26), which are highly conserved across species (41). Interestingly, the human FcRn receptor is very stringent in its ligand specificity, as it does not bind murine IgG1 and IgG2a. A recent explanation of this phenomenon suggests the existence of specific docking sites that are defined by variations in contacts between residues for different FcRn-IgG pairs (42). Thus, although the information gathered from the biodistributions is valuable in understanding how a particular mutation in the Fc region affects the antibody fragment half-life and which mutation is more effective in reducing circulation persistence, the murine system is not ideal. Direct measurement of the absolute binding affinity of our scFv-Fc fragments for the human FcRn receptor could provide a better estimation of the kinetic properties that these fragments might exhibit if introduced into a human system. In addition, an existing human FcRn transgenic mouse model (43) should prove informative in predicting the behavior of antibody fragments in clinical use.

The use of radioiodine as the label in the current studies allowed primarily for obtaining blood clearance and tumor targeting data. However, it provides little information on normal organ clearance, as iodide and iodotyrosine are released and cleared quickly following endocytosis and catabolism. The substitution of radioiodine with radiometal, such as $^{111}In$, conjugated via the use of a chelate, will provide insight into the involvement of normal organs in the metabolism of the radiolabeled scFv-Fc fragments. Such experiments are in progress, and preliminary data suggest that the main clearance route of scFv-Fc fragments is via the liver, as expected considering their molecular size.

*In vivo* imaging by microPET allowed rapid evaluation of the target and biodistribution of the radiolabeled scFv-Fc fragments in tumor-bearing mice. The microPET images provided us with a sensitive method for visualization of tumor masses; however, accurate quantitation of $^{124}I$ from the small animal scans is not feasible yet due to its complex decay scheme (44). Therefore, we evaluated the targeting potential of scFv-Fc by examining

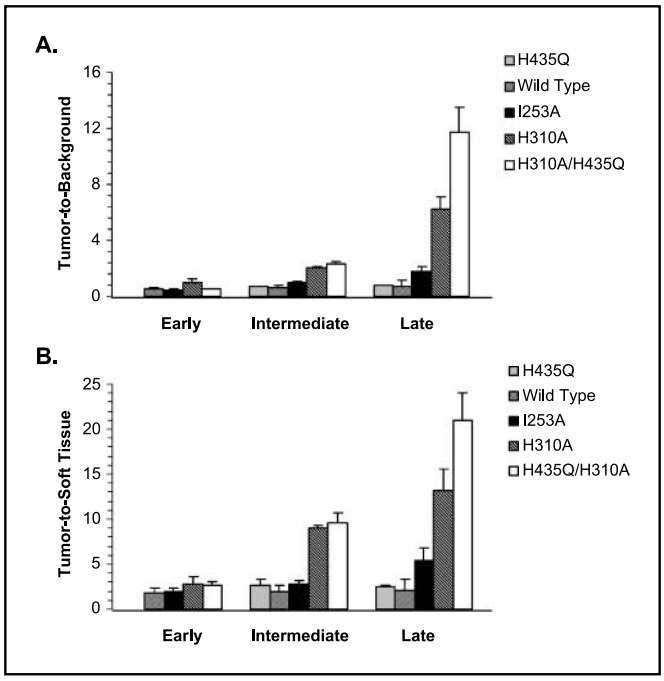


**Figure 6.** *A,* ratios derived from the PET data comparing CEA-positive tumor-to-background levels of $^{124}I$ activity. Early (3-4 hours), intermediate (16-18 hours), and late (48-90 hours) time points. *B,* ratios derived from the PET data comparing CEA-positive tumor-to-soft tissue levels of $^{124}I$ activity.

tumor-to-nontarget ratios from the images. Both the images and the calculated tumor-to-nontarget ratios confirmed that H310A/H435Q quickly localizes to the tumor site and clears rapidly from the circulation, resulting in the best images, followed by the other fast clearing scFv-Fc construct (H310A). The I253A, H435Q, and wild-type scFv-Fc were eliminated at a slower rate and achieved higher activity levels in the CEA-positive tumor (biodistribution data following the microPET scans), but the background radioactivity took longer to clear and was still apparent at 18 hours postinjection. In contrast, the radioactivity delivered to the CEA-positive xenografts by scFv-Fc H310A and the H310A/H435Q mutants was lower; however, there was virtually no background activity seen in the mouse at the intermediate and final scans.

Among the scFv-Fc proteins used in the imaging studies, the H310A/H435Q mutant showed a superior ability to quickly localize to the tumor site and clear from the circulation, thus producing clear, high-contrast images at early time points. The slow (wild-type and H435Q) and intermediate (I253A and H310A) clearing fragments provide a spectrum of candidates that could be more suitable for specific therapy or imaging applications. Ongoing studies of radiometal-labeled fragments (including $^{64}$Cu microPET imaging) will provide quantitative data on tumor localization and primary organ clearance in the live animal. The approach documented here should be applicable to engineering of additional antibodies or Fc fusion proteins for development of agents with controlled pharmacokinetic properties.

## Summary

The work summarized here suggests that, in addition to functional domain deletions, one can manipulate the terminal biological half-life and mean residence time of recombinant antibody fragments through modulating the interaction with the protective FcRn receptor. The introduction of specific mutations at the FcRn-Fc interface resulted in the generation of several antibody fragments with the same size and format, exhibiting significantly different clearance kinetics. The introduced mutations did not interfere with protein expression and localization to the tumor. Specifically, the I253A and H310A variants could be of interest in conjugation to therapeutic agents, such as $^{90}$Y, whereas the H310A/H435Q double mutant could be used in imaging applications.

## Acknowledgments

Received 7/20/2004; revised 9/22/2004; accepted 11/11/2004.

**Grant support:** NIH grants CA 43904 and CA 86306 and Department of the Army grants DAMD 17-00-1-203 and DAMD 17-00-1-0150. L.E. Williams, J.E. Shively, A.A. Raubitschek, and A.M. Wu are members of the City of Hope Comprehensive Cancer Center (NIH CA 33572). S.S. Gambhir and A.M. Wu are members of the University of California, Los Angeles Jonsson Comprehensive Cancer Center (NIH CA 16042).

The costs of publication of this article were defrayed in part by the payment of page charges. This article must therefore be hereby marked advertisement in accordance with 18 U.S.C. Section 1734 solely to indicate this fact.

We thank Anne-Line Anderson and Randall Woo for $^{125}$I/$^{131}$I labeling of the engineered proteins, Militza Bocic for the analysis of immunoreactivity, Xiaoman Lewis for $^{124}$I-scFv-Fc injections, Judy Edwards and Waldemar Ladno for assistance with the microPET scans, and Andy Loening who helped in the image production.



## References

1. Hu S, Shively L, Raubitschek A, et al. Minibody: a novel engineered anti-carcinoembryonic antigen antibody fragment (single-chain Fv-CH3) which exhibits rapid, high-level targeting of xenografts. Cancer Res 1996;56: 3055–61.
2. Wu AM, Yazaki PJ. Designer genes: recombinant antibody fragments for biological imaging. Q J Nucl Med 2000;44:268–83.
3. Yazaki PJ, Wu AM, Tsai SW, et al. Tumor targeting of radiometal labeled anti-CEA recombinant T84.66 diabody and T84.66 minibody: comparison to radioiodinated fragments. Bioconjug Chem 2001;12:220–8.
4. Slavin-Chiorini DC, Kashmiri SV, Schlom J, et al. Biological properties of chimeric domain-deleted anticarcinoma immunoglobulins. Cancer Res 1995;55: 5957–67S.
5. Xu X, Clarke P, Szalai G, et al. Targeting and therapy of carcinoembryonic antigen-expressing tumors in transgenic mice with an antibody-interleukin 2 fusion protein. Cancer Res 2000;60:4475–84.
6. Kim JK, Tsen MF, Ghetie V, Ward ES. Catabolism of the murine IgG1 molecule: evidence that both $C_H2$-$C_H3$ domain interfaces are required for persistence of IgG1 in the circulation of mice. Scand J Immunol 1994;40: 457–65.
7. Brambell FW. The transmission of immunity from mother to young and the catabolism of immunoglobulins. Lancet 1966;2:1087–93.
8. Ghetie V, Hubbard JG, Kim JK, Tsen MF, Lee Y, Ward ES. Abnormally short serum half-lives of IgG in $\beta_2$-microglobulin-deficient mice. Eur J Immunol 1996;26:690–6.
9. Junghans RP, Anderson CL. The protection receptor for IgG catabolism is the $\beta_2$-microglobulin-containing neonatal intestinal transport receptor. Proc Natl Acad Sci U S A 1996;93:5512–6.
10. Israel EJ, Wilsker DF, Hayes KC, Schoenfeld D, Simister NE. Increased clearance of IgG in mice that lack $\beta_2$-microglobulin: possible protective role of FcRn. Immunology 1996;89:573–8.
11. Brambell FWR, Halliday R, Morris IG. Interference by human and bovine serum and serum protein fractions with the absorption of antibodies by suckling rats and mice. Proc R Soc Lond B Biol Sci 1958; 149:1–11.
12. Rodewald R. Selective antibody transport in the proximal small intestine of the neonatal rat. J Cell Biol 1970;45:635–40.
13. Simister NE, Mostov KE. An Fc receptor structurally related to MHC class I antigens. Nature 1989; 337:184–7.
14. Ahouse JJ, Hagerman CL, Mittal P, et al. Mouse MHC class I-like Fc receptor encoded outside the MHC. J Immunol 1993;151:6076–88.
15. Brambell FWR. The transmission of immune globulins from the mother to young. Amsterdam: North Holland Publishing; 1970.
16. Waldmann TA, Strober W. Metabolism of immunoglobulins. Prog Allergy 1969;13:1–110.
17. Junghans RP. Finally! The Brambell receptor (FcRB). Mediator of transmission of immunity and protection from catabolism for IgG. Immunol Res 1997;16:29–57.
18. Rodewald R. pH-dependent binding of immunoglobulins to intestinal cells of the neonatal rat. J Cell Biol 1976;71:666–9.
19. Simister NE, Rees AR. Isolation and characterization of an Fc receptor from neonatal rat small intestine. Eur J Immunol 1985;15:733–8.
20. Ghetie V, Ward ES. Multiple roles for the major histocompatibility complex class I-related receptor FcRn. Annu Rev Immunol 2000;18:739–66.
21. Medesan C, Matesoi D, Radu C, Ghetie V, Ward ES. Delineation of the amino acid residues involved in transcytosis and catabolism of mouse IgG1. J Immunol 1997;158:2211–7.
22. Kim JK, Firan M, Radu CG, Kim CH, Ghetie V, Ward ES. Mapping the site on human IgG for binding of the MHC class I-related receptor, FcRn. Eur J Immunol 1999;29:2819–25.
23. Shields RL, Namenuk AK, Hong K, et al. High resolution mapping of the binding site on human IgG1 for FcγRI, FcγRII, FcγRIII, and FcRn and design of IgG1 variants with improved binding to the FcγR. J Biol Chem 2001;276:6591–604.
24. Hornick JL, Sharifi J, Khawli LA, et al. Single amino acid substitution in the Fc region of chimeric TNT-3 antibody accelerates clearance and improves immunoscintigraphy of solid tumors. J Nucl Med 2000;41:355–62.
25. West AP Jr, Bjorkman PJ. Crystal structure and immunoglobulin G binding properties of the human major histocompatibility complex-related Fc receptor(,). Biochemistry 2000;39:9698–708.
26. Martin WL, West AP Jr, Gan L, Bjorkman PJ. Crystal structure at 2.8 A of an FcRn/heterodimeric Fc complex: mechanism of pH-dependent binding. Mol Cell 2001;7: 867–77.
27. Ghetie V, Popov S, Borvak J, et al. Increasing the serum persistence of an IgG fragment by random mutagenesis. Nat Biotechnol 1997;15:637–40.
28. Hinton PR, Johlfs MG, Xiong JM, et al. Engineered human IgG antibodies with longer serum half-lives in primates. J Biol Chem 2004;279:6213–6.
29. Bebbington CR, Renner G, Thomson S, King D, Abrams D, Yarranton GT. High-level expression of a recombinant antibody from myeloma cells using a glutamine synthetase gene as an amplifiable selectable marker. Biotechnology (N Y) 1992;10:169–75.
30. Galfre G, Milstein C. Preparation of monoclonal antibodies: strategies and procedures. Methods Enzymol 1981;73:3–46.
31. Yazaki PJ, Shively L, Clark C, et al. Mammalian expression and hollow fiber bioreactor production of recombinant anti-CEA diabody and minibody for clinical applications. J Immunol Methods 2001;253: 195–208.

**32.** Olafsen T, Cheung CW, Yazaki PJ, et al. Covalent disulfide-linked anti-CEA diabody allows site-specific conjugation and radiolabeling for tumor targeting applications. Protein Eng Des Sel 2004;17:21–7.

**33.** Wu AM, Williams LE, Zieran L, et al. Anti-carcinoembryonic antigen (CEA) diabody for rapid tumor targeting and imaging. Tumor Targeting 1999;4:47–58.

**34.** D'Argenio DZ, Schumitzky A. A program package for simulation and parameter estimation in pharmacokinetic systems. Comput Programs Biomed 1979;9:115–34.

**35.** Defrise M, Kinahan PE, Townsend DW, Michel C, Sibomana M, Newport DF. Exact and approximate rebinning algorithms for 3-D PET data. IEEE Trans Med Imaging 1997;16:145–58.

**36.** Loening AM, Gambhir SS. AMIDE: a free software tool for multimodality medical image analysis. Mol Imaging 2003;2:131–7.

**37.** Deisenhofer J. Crystallographic refinement and atomic models of a human Fc fragment and its complex with fragment B of protein A from *Staphylococcus aureus* at 2.9- and 2.8-A resolution. Biochemistry 1981;20:2361–70.

**38.** Benet LZ, Galeazzi RL. Noncompartmental determination of the steady-state volume of distribution. J Pharm Sci 1979;68:1071–4.

**39.** Williams LE, Wu AM, Yazaki PJ, et al. Numerical selection of optimal tumor imaging agents with application to engineered antibodies. Cancer Biother Radiopharm 2001;16:25–35.

**40.** Ober RJ, Radu CG, Ghetie V, Ward ES. Differences in promiscuity for antibody-FcRn interactions across species: implications for therapeutic antibodies. Int Immunol 2001;13:1551–9.

**41.** Kabat EA, Wu TT, Perry HM, Gottesman KS, Foeller C. Sequences of proteins of immunological interest. U.S. Department of Health and Human Services edition. Bethesda: Public Health Service NIH; 1991.

**42.** Zhou J, Johnson JE, Ghetie V, Ober RJ, Sally Ward E. Generation of mutated variants of the human form of the MHC class I-related receptor, FcRn, with increased affinity for mouse immunoglobulin G. J Mol Biol 2003;332:901–13.

**43.** Roopenian DC, Christianson GJ, Sproule TJ, et al. The MHC class I-like IgG receptor controls perinatal IgG transport, IgG homeostasis, and fate of IgG-Fc-coupled drugs. J Immunol 2003;170:3528–33.

**44.** Sundaresan G, Yazaki PJ, Shively JE, et al. $^{124}$I-labeled engineered anti-CEA minibodies and diabodies allow high-contrast, antigen-specific small-animal PET imaging of xenografts in athymic mice. J Nucl Med 2003;44:1962–9.

**45.** Neumaier M, Shively L, Chen FS, et al. Cloning of the genes for T84.66, an antibody that has a high specificity and affinity for carcinoembryonic antigen, and expression of chimeric human/mouse T84.66 genes in myeloma and Chinese hamster ovary cells. Cancer Res 1990;50:2128–34.